AIMS Mathematics, 11(3): 5532–5556.
DOI: 10.3934/math.2026228
Received: 08 October 2025
Revised: 01 February 2026
Accepted: 04 February 2026
Published: 04 March 2026

https://www.aimspress.com/journal/Math

Research article

Exact traveling wave solutions for the Chafee-Infante equation via a generalized first integral method

Muhammad Noman Qureshi[1,*], Atif Hassan Soori[1], Muhammad Shoaib Arif[2] and Kamaleldin Abodayeh[2]

[1] Department of Mathematics, Faculty of Basic and Applied Sciences, Air University, Islamabad, Pakistan

[2] Department of Mathematics and Sciences, College of Sciences and Humanities, Prince Sultan University, Riyadh, Saudia Arabia

* **Correspondence:** Email: 211900@students.au.edu.pk; +923121577115.

Abstract: This study derives novel exact traveling wave solutions for the nonlinear (1+1)-dimensional Chafee-Infante equation by synthesizing the generalized first integral method (GFIM) with Laurent polynomial expansions. As a fundamental reaction-diffusion model, the Chafee-Infante equation governs pattern formation in diverse systems—from biological to chemical and physical contexts—yet its strong nonlinearity poses persistent challenges to classical integration techniques such as the inverse scattering transform or Hirota's method. We transform the equation into an autonomous polynomial system and employ the division theorem to systematically identify its first integrals, thereby circumventing the need for auxiliary equations or ansatz-based heuristics. By introducing Laurent polynomial ansatzes of varying complexity—ranging from first-degree to higher-order expansions—we yield compact rational-exponential solutions that are both exact and computationally tractable. The validity of these solutions is confirmed through symbolic computation in Mathematica, while a detailed graphical analysis elucidates their behavior—from bounded, dissipative profiles to singular structures—across different parameter regimes, including the critical thresholds $C = 0$ and $C = 2$ where blow-up phenomena emerge. This work underscores the efficacy of merging Laurent series with algebraic methods, offering a powerful and generalized tool for extracting exact solutions from a broader class of intractable nonlinear partial differential equations (PDEs) arising in mathematical physics and applied mathematics.

Keywords: Chafee-Infante equation; exact solutions; generalized first integral method; Laurent polynomial ansatz; polynomial differential systems; division theorem; traveling waves
Mathematics Subject Classification: 35Q53, 35C07, 35B40, 35B35, 35A25, 35Q51, 35G20

1. Introduction

The (1 + 1)-dimensional Chafee–Infante equation represents a cornerstone reaction-diffusion model with broad applications across biology, chemistry, and physics. This equation captures the spatiotemporal dynamics of systems where diffusion interacts with nonlinear reactions, and is given by

$$U_t - U_{xx} + \lambda(U^3 - U) = 0, \tag{1.1}$$

where $U(x, t)$ denotes a state variable—for example, concentration, temperature, or population density—whose interpretation depends on the specific application. Here, U_t expresses the temporal rate of change, U_{xx} models spatial diffusion, and the parameter $\lambda > 0$ is a fixed constant that controls the interplay between linear and nonlinear effects, thereby playing a critical role in the overall system behavior [10, 11, 32].

This study focuses on traveling wave solutions propagating along infinite domains ($x \in (-\infty, \infty)$), which naturally satisfy vanishing boundary conditions at infinity. While boundary conditions play a crucial role in confined systems, our analytical approach targets the intrinsic wave structures of the equation itself.

A key feature of the Chafee-Infante equation is its ability to model pattern formation. It helps explain the development of spatially periodic structures and traveling fronts in various contexts, such as population genetics, combustion waves, and phase separation in materials [13, 21, 28]. In each case, the competition between diffusion and nonlinearity produces rich and complex spatiotemporal evolution. Understanding its solution set is therefore crucial for progress in both theoretical and applied nonlinear dynamics.

Given the equation's importance, researchers have developed a wide range of analytical and numerical methods to construct exact solutions. Well-known techniques include the tanh-sech method [8], the extended tanh approach [3], the sine-cosine method [7], and the first integral method (FIM) [1]. The FIM, in particular, offers a powerful algebraic framework for deriving exact traveling wave solutions. It is valued for its ability to produce explicit, high-precision results while avoiding overly tedious computations [5, 6, 16]. Variants and extensions of the FIM have been successfully applied to other important equations, such as the Konopelchenko–Dubrovsky equation [2] and various conformable fractional differential equations [5].

However, the classical FIM is typically limited to standard polynomial ansatze and often fails to capture solutions with singularities or more complex functional structures. This limitation has motivated the development of generalized approaches [3, 20, 30]. More recently, methods such as generalized expansion techniques [17], stochastic soliton solutions [18], and advanced dynamical systems analyses [29] have further expanded our ability to analyze nonlinear partial differential equations (PDEs). In parallel, novel solution frameworks like the unified ansätze approach [4], the Exp-function method [9], and the power index method [12,22] have been employed to tackle equations arising in mathematical biology, optics, and fluid dynamics [14, 15, 27].

It is important to note that not all nonlinear PDEs admit closed-form exact solutions, and many real-world problems ultimately require numerical treatment. However, for equations that are amenable to analytical methods—such as the Chafee–Infante equation with its polynomial nonlinearity—the derivation of exact solutions provides invaluable insight into the system's fundamental behavior, serves as benchmarks for numerical schemes, and reveals parameter regimes of particular interest.

In situations where purely analytical solutions are difficult to obtain, numerical methods—including finite difference schemes [23, 24] and hybrid analytical-numerical techniques [19]—provide valuable complementary insights. The structure of the paper is organized as follows:

- **Section 2:** Provides a concise yet comprehensive overview of the generalized first integral method, detailing its theoretical foundation and applicability.
- **Section 3:** Demonstrates the application of the method to derive exact solutions of the (1 + 1)-dimensional Chafee–Infante equation, including step-by-step calculations for different Laurent polynomial orders.
- **Section 4:** Discusses the mathematical and physical implications of the derived solutions, emphasizing their behavior and parameter effects.
- **Section 5:** Presents graphical illustrations of the solution profiles, highlighting key features and behaviors under varying parameters.
- **Section 6:** Summarizes the principal findings of the study and outlines potential avenues for future research.

2. Structural layout of the generalized first integral method

The generalized first integral method (GFIM) proceeds through four systematic steps, beginning with the reduction of the governing PDE to an ordinary differential equation and culminating in the construction of exact traveling wave solutions. Each step is elaborated below.

2.1. Step 1: Reduction of the PDE to an ODE via traveling wave transformation

Consider a general nonlinear partial differential equation (PDE) of the form

$$E(U, U_x, U_t, U_{xx}, U_{xt}, \dots) = 0, \tag{2.1}$$

where $U = U(x, t)$ is an unknown function and the subscripts denote partial derivatives, for example,

$$U_x = \frac{\partial U}{\partial x}, \; U_t = \frac{\partial U}{\partial t}, \text{ etc.}$$

To seek traveling wave solutions, we introduce the wave variable

$$\xi = x - ct, \tag{2.2}$$

where c is the wave speed to be determined. This transformation reduces the PDE to an ordinary differential equation (ODE) by assuming the solution has the form

$$U(x, t) = U(\xi), \tag{2.3}$$

i.e., the solution profile depends only on the traveling coordinate ξ.

Using the chain rule, we compute the partial derivatives of $U(x, t)$ with respect to x and t in terms of ξ as follows:

$$\frac{\partial U}{\partial x} = \frac{dU}{d\xi} \cdot \frac{d\xi}{dx} = \frac{dU}{d\xi}, \tag{2.4}$$

$$\frac{\partial U}{\partial t} = \frac{dU}{d\xi} \cdot \frac{d\xi}{dt} = -c\frac{dU}{d\xi}, \tag{2.5}$$

$$\frac{\partial^2 U}{\partial x^2} = \frac{d}{dx}\left(\frac{\partial U}{\partial x}\right) = \frac{d}{d\xi}\left(\frac{dU}{d\xi}\right)\cdot\frac{d\xi}{dx} = \frac{d^2U}{d\xi^2}, \tag{2.6}$$

$$\frac{\partial^2 U}{\partial t\partial x} = \frac{d}{dt}\left(\frac{\partial U}{\partial x}\right) = \frac{d}{d\xi}\left(\frac{dU}{d\xi}\right)\cdot\frac{d\xi}{dt} = -c\frac{d^2U}{d\xi^2}, \tag{2.7}$$

and similarly for all higher-order partial derivatives, applying the chain rule iteratively.

Substituting these expressions into the original PDE (2.1), the equation is converted into an ordinary differential equation (ODE) of the form

$$F\left(U, \frac{dU}{d\xi}, \frac{d^2U}{d\xi^2}, \ldots\right) = 0, \tag{2.8}$$

where $U = U(\xi)$ is now a function of a single independent variable ξ, and F is typically a polynomial or rational function in U and its derivatives.

2.2. Step 2: Transformation to a polynomial autonomous system

Assuming that the function $U(\xi)$ is sufficiently smooth, we define new dependent variables to convert the higher-order ODE into a system of first-order equations:

$$X(\xi) = U(\xi), \quad Y(\xi) = \frac{dU}{d\xi}. \tag{2.9}$$

Differentiating $X(\xi)$ with respect to ξ, we have

$$\frac{dX}{d\xi} = \frac{dU}{d\xi} = Y(\xi), \tag{2.10}$$

$$\frac{dY}{d\xi} = \frac{d^2U}{d\xi^2} = G(X, Y), \tag{2.11}$$

where $G(X, Y)$ is a nonlinear algebraic function obtained from the transformed form of the original PDE. The resulting system (2.10) and (2.11) is a polynomial autonomous system in the phase variables (X, Y).

2.3. Step 3: Construction of first integrals via Laurent polynomials and division theorem

Once the polynomial autonomous system is obtained, the next step is to find one or more first integrals of the system. A first integral is a function $I(X, Y)$ that remains constant along solutions of the system, i.e., $\frac{dI}{d\xi} = 0$. In many nonlinear systems, standard methods fail to construct first integrals. To address this, the division theorem for Laurent polynomials is applied in the generalized first integral method. Laurent polynomials are generalized polynomials that include both positive and negative powers of variables. This extended structure allows for richer expressions and more flexibility in representing invariants compared to standard polynomials—a key advantage that enables the discovery of more complex solution structures.

An ansatz for the first integral is proposed in the following form:

$$I(X, Y) = \sum_{(m,n)\in S} a_{mn} X^m Y^n, \tag{2.12}$$

where $S \subset \mathbb{Z}^2$ is a finite index set and $a_{mn} \in \mathbb{R}$ (or $\mathbb{C}$) are unknown coefficients to be determined. The choice of the index set S, particularly the range of n (denoted by β), determines the complexity of the solution structure that can be obtained. While simpler choices like $\beta = 1$ yield tractable systems and elementary solutions, higher values such as $\beta = 2$ can reveal more abundant and complex solution families.

Substituting $I(X, Y)$ into the total derivative along the system's flow and enforcing $\frac{dI}{d\xi} = 0$, we obtain an algebraic condition:

$$\frac{dI}{d\xi} = \frac{\partial I}{\partial X}\frac{dX}{d\xi} + \frac{\partial I}{\partial Y}\frac{dY}{d\xi} = \frac{\partial I}{\partial X}Y + \frac{\partial I}{\partial Y}G(X, Y) = 0. \tag{2.13}$$

This equation is then simplified and equated term-by-term to zero to obtain a system of algebraic equations in the coefficients a_{mn}. Solving this system provides the explicit form of the first integral $I(X, Y)$.

The existence of an exact solution via this method is not guaranteed a priori but is established through the consistency of the resulting algebraic system. If a non-trivial solution for the coefficients a_{mn} exists that satisfies all algebraic constraints, then the reduced system is guaranteed to be integrable, yielding an exact solution to the original PDE.

Once a first integral is known, the order of the system is reduced. In particular, the second-order ODE (2.8) is effectively converted into a first-order integrable ODE via the first integral:

$$I(X, Y) = C, \tag{2.14}$$

where C is a constant of integration. Solving this reduced equation yields the explicit analytical form of $U(\xi)$, and therefore provides the exact traveling wave solution of the original PDE (2.1).

2.4. Step 4: Summary of the method

In summary, the generalized first integral method provides a systematic and algebraic framework to derive exact solutions of nonlinear PDEs by

- transforming the PDE into an ODE via traveling wave substitution,
- reformulating the ODE as a polynomial autonomous system,
- applying the division theorem for Laurent polynomials to construct conserved quantities (first integrals),
- and solving the reduced system to obtain exact solutions.

3. Flowchart of the generalized first integral method

Table 1 presents a systematic flowchart outlining the key steps of the generalized first integral method for deriving exact traveling wave solutions. The procedure begins with the given PDE and sequentially applies a traveling wave reduction, transformation to an autonomous dynamical system, and construction of a first integral via the division theorem for Laurent polynomials. This first integral is then used to reduce the order of the system, ultimately yielding the exact solution. The flowchart provides a clear, replicable framework for applying the method to a wide class of nonlinear evolution equations.

Table 1. Flowchart illustrating the step-by-step procedure of the generalized first integral method for obtaining exact traveling wave solutions.

Start with PDE

$E(U, U_x, U_t, U_{xx}, U_{xt}, \ldots) = 0$

$\Downarrow$

Step 1: Traveling wave reduction

$\xi = x - ct$, $U(x,t) = U(\xi)$

Reduce PDE to ODE: $F(U, U', U'', \ldots) = 0$

$\Downarrow$

Step 2: Autonomous system

$X = U$, $Y = U'$

$X' = Y$, $Y' = G(X, Y)$

$\Downarrow$

Step 3: First integral construction

Apply division theorem for Laurent polynomials

Find $I(X, Y)$ such that $\dfrac{dI}{d\xi} = 0$

$\Downarrow$

Step 4: Reduction and solution

Use $I(X, Y) = C$ to reduce order

Solve for $U(\xi)$

$\Downarrow$

Exact traveling wave solution

$U(x,t) = U(\xi)$ with $\xi = x - ct$

4. Mathematical foundation

Theorem 1. *(Division theorem for Laurent polynomials) Let $P(\omega, z)$ and $Q(\omega, z)$ be two Laurent polynomials in the field $\mathbb{C}(\omega, z)$, where $\mathbb{C}$ denotes the set of complex numbers. Suppose that $P(\omega, z)$ is irreducible in the polynomial ring $\mathbb{C}[\omega, z]$. If $Q(\omega, z)$ vanishes at every common zero of $P(\omega, z)$, that is,*

$$Q(\omega, z) = 0 \quad \textit{whenever} \quad P(\omega, z) = 0, \tag{4.1}$$

then there exists a Laurent polynomial $G(\omega, z) \in \mathbb{C}[\omega, z]$ such that

$$Q(\omega, z) = P(\omega, z) \cdot G(\omega, z). \tag{4.2}$$

In other words, $P(\omega, z)$ divides $Q(\omega, z)$ in the ring of Laurent polynomials over $\mathbb{C}$. This result plays a fundamental role in constructing first integrals of polynomial differential systems by enabling the factorization of expressions involving multiple variables.

5. Application of the generalized first integral method to a nonlinear partial differential equation

Consider the (1 + 1)-dimensional Chafee–Infante equation given by

$$U_t - U_{xx} + \lambda(U^3 - U) = 0, \tag{5.1}$$

where λ is a real parameter. To seek traveling-wave solutions, we introduce the general traveling-wave transformation:

$$\xi = x - ct, \tag{5.2}$$

with c denoting the (real) wave speed to be determined. Assuming a solution of the form

$$U(x, t) = f(\xi), \tag{5.3}$$

and applying the chain rule, we obtain

$$U_t = -cf'(\xi), \qquad U_{xx} = f''(\xi). \tag{5.4}$$

Substituting these expressions into Eq (5.1) yields the following second-order autonomous ordinary differential equation:

$$f''(\xi) + c\, f'(\xi) + \lambda f(\xi) - \lambda f^3(\xi) = 0. \tag{5.5}$$

5.1. Reduction to an autonomous system

Here, we introduce the following phase-plane variables:

$$X(\xi) = f(\xi), \qquad Y(\xi) = f'(\xi). \tag{5.6}$$

Equation (5.5) can be written as the following two-dimensional polynomial autonomous system:

$$\frac{dX}{d\xi} = Y, \tag{5.7}$$

$$\frac{dY}{d\xi} = -\,c\,Y - \lambda X + \lambda X^3. \tag{5.8}$$

Remark. System (5.7) and (5.8) constitutes an autonomous polynomial dynamical system in the phase plane (X, Y). The search for its first integral $I(X, Y)$—a conserved quantity satisfying $\frac{dI}{d\xi} = 0$ along solution trajectories—allows the reduction of the system to a first-order ODE $I(X, Y) = C$, from which exact traveling-wave solutions $U(\xi)$ of the original PDE can be obtained.

5.2. Methodology overview

The generalized first integral method (GFIM) with a Laurent-polynomial ansatz imposes algebraic consistency conditions on the coefficients of the ansatz and on the system parameters. These conditions ensure the existence of a non-trivial first integral and are examined separately in each case below. In the following subsections, we illustrate the method for two concrete choices of the Laurent-polynomial order.

For clarity of presentation, we first fix the wave speed $c = -1$; the analysis for $c = +1$ follows analogous steps and leads to a corresponding family of traveling-wave solutions propagating in the opposite direction. With $c = -1$, system (5.7) and (5.8) reduces to

$$\frac{dX}{d\xi} = Y, \tag{5.9}$$

$$\frac{dY}{d\xi} = Y + \lambda X^3 - \lambda X, \tag{5.10}$$

which coincides with the system obtained by the traveling-wave transformation $\xi = x + t$ applied to the original PDE.

Applying the GFIM with different orders of the Laurent-polynomial ansatz leads, in each case, to an overdetermined algebraic system for the unknown coefficients. The admissible values of the parameter λ then arise naturally from the solvability conditions of these systems and are discussed explicitly within the corresponding cases.

5.3. Solution via first-order Laurent polynomial ansatz ($\beta = 1$)

We begin with a first-order Laurent polynomial ansatz to demonstrate the fundamental methodology. This choice of $\beta = 1$ provides a tractable system that yields elementary solutions while illustrating the core approach.

Suppose $X(\xi)$ and $Y(\xi)$ are non-trivial solutions of Eq (3.4). Let

$$I(X, Y) = \sum_{k=\alpha}^{\beta} a_k(X) Y^k, \tag{5.11}$$

be an irreducible Laurent polynomial in $\mathbb{C}[X(\xi), Y(\xi)]$ such that

$$I[X(\xi), Y(\xi)] = \sum_{k=\alpha}^{\beta} a_k(X) Y^k = 0, \tag{5.12}$$

where $a_k(X) \in \mathbb{C}[X, X^{-1}]$ are Laurent polynomials. The expression in Eq (5.12) is said to be a first integral of Eqs (5.9) and (5.10).

By applying the division theorem, there exists a Laurent polynomial of the form $[g(X) + h(X)Y] \in \mathbb{C}[X, Y]$ such that, by the chain rule,

$$\frac{dI}{d\xi} = \sum_{k=\alpha}^{\beta} a_k'(X) Y^{k+1} + \sum_{k=\alpha}^{\beta} k a_k(X) Y^k + (\lambda X^3 - \lambda X) \sum_{k=\alpha}^{\beta} k a_k(X) Y^{k-1}, \tag{5.13}$$

$$[g(X) + h(X)Y] \cdot \left(\sum_{k=\alpha}^{\beta} a_k(X) Y^k \right) = \sum_{k=\alpha}^{\beta} a_k'(X) Y^{k+1} + \sum_{k=\alpha}^{\beta} k a_k(X) Y^k + (\lambda X^3 - \lambda X) \sum_{k=\alpha}^{\beta} k a_k(X) Y^{k-1}. \quad (5.14)$$

Remark. The division theorem guarantees the existence of Laurent polynomials $g(X)$ and $h(X)$ such that the total derivative $\frac{dI}{d\xi}$ factors as $[g(X) + h(X)Y] \cdot I$. Equating coefficients of powers of Y yields the following algebraic conditions.

Now, for $\alpha = 0$ and $\beta = 1$, Eq (5.14) becomes

$$[g(X) + h(X)Y] \cdot (a_0(X) + a_1(X)Y) = a_0'(X)Y + a_1'(X)Y^2 + a_1(X)Y + a_1(X)(\lambda X^3 - \lambda X). \quad (5.15)$$

Compare coefficients of powers of Y from both sides:

Coefficient of Y^2:

$$h(X)a_1(X) = a_1'(X). \quad (5.16)$$

Coefficient of Y^1:

$$h(X)a_0(X) + g(X)a_1(X) = a_0'(X) + a_1(X). \quad (5.17)$$

Coefficient of Y^0:

$$g(X)a_0(X) = a_1(X)(\lambda X^3 - \lambda X). \quad (5.18)$$

From Eq (5.16), we suppose that

$$h(X) = \frac{1}{X}. \quad (5.19)$$

Substitute into Eq (5.16):

$$\frac{1}{X} = \frac{a_1'(X)}{a_1(X)}.$$

Integrate both sides:

$$a_1(X) = C_1 X. \quad (5.20)$$

Substitute into Eq (5.17):

$$\frac{a_0(X)}{X} + C_1 X g(X) = a_0'(X) + C_1 X.$$

Rewrite as

$$C_1 X g(X) - C_1 X = a_0'(X) - \frac{a_0(X)}{X},$$

$$C_1 g(X) - C_1 = \frac{d}{dX}\left(\frac{a_0(X)}{X}\right).$$

Integrate both sides:

$$C_1 \int g(X)\, dX - C_1 X + C_2 = \frac{a_0(X)}{X},$$

$$a_0(X) = C_1 X \int g(X)\, dX - C_1 X^2 + C_2 X. \quad (5.21)$$

Substitute Eqs (5.20) and (5.21) into Eq (5.18):

$$[C_1X \int g(X)\,dX - C_1X^2 + C_2X] \cdot g(X) = C_1X(\lambda X^3 - \lambda X).$$

Divide by C_1 and rearrange:

$$g(X) \int g(X)\,dX - Xg(X) + Ag(X) = \lambda X^3 - \lambda X,$$

where $A = \dfrac{C_2}{C_1}$.

We assume $g(X) = aX + b$, a linear form, in order to balance the degree of the polynomial terms on both sides of the equation, ensuring that the structure of the system remains algebraically consistent and solvable within the Laurent polynomial framework. Then,

$$(aX + b) \int (aX + b)\,dX - X(aX + b) + A(aX + b) = \lambda X^3 - \lambda X,$$
$$(aX + b)\left(\frac{aX^2}{2} + bX + C\right) - X(aX + b) + A(aX + b) = \lambda X^3 - \lambda X.$$

Expand and compare powers of X:

Coefficient of X^3:

$$\frac{a^2}{2} = \lambda \quad \Rightarrow \quad a = \sqrt{2\lambda}.$$

Coefficient of X^2:

$$\frac{3ab}{2} - a = 0 \quad \Rightarrow \quad b = \frac{2}{3}, \quad \text{since } a \neq 0.$$

Coefficient of X^1:

$$aC + b^2 - b + Aab = -\lambda.$$

Using $a = \sqrt{2\lambda}$ and $b = \frac{2}{3}$, we obtain

$$\frac{4}{9} - \frac{2}{3} + A\sqrt{2\lambda} \cdot \frac{2}{3} = -\lambda.$$

Coefficient of X^0:

$$Ab = 0 \quad \Rightarrow \quad A = 0 \quad (\text{as } b \neq 0),$$
$$\Rightarrow -\frac{2}{9} = -\lambda \quad \Rightarrow \quad \lambda = \frac{2}{9}.$$

Justification of the parameter constraint. The specific value $\lambda = \frac{2}{9}$ emerges as a necessary condition for the existence of a non-trivial Laurent-polynomial first integral within the $\beta = 1$ ansatz. The algebraic system obtained from equating coefficients of powers of Y is overdetermined; its solvability forces λ to take exactly this value. Any other value would lead to an inconsistent system with only the trivial solution $a_{mn} = 0$. Thus, $\lambda = \frac{2}{9}$ is not an arbitrary choice but a direct consequence of the integrability structure detected by the GFIM. Thus, we find

$$g(X) = aX + b = \sqrt{2\lambda}\, X + \frac{2}{3} = \frac{2}{3}(X + 1). \tag{5.22}$$

Using Eq (5.18), we get

$$a_0(X)\left[\frac{2}{3}(X + 1)\right] = C_1 X(\lambda X^3 - \lambda X). \tag{5.23}$$

Solve for $a_0(X)$:

$$a_0(X) = \frac{C_1 X(\lambda X^3 - \lambda X)}{\frac{2}{3}(X + 1)}.$$

$$a_0(X) = \frac{C_1(X^4 - X^2)}{3(X + 1)},$$

where $\lambda = \frac{2}{9}$. Now, from Eq (5.12), we get

$$a_0(X) + a_1(X)Y = 0 \quad \Rightarrow \quad Y = -\frac{a_0(X)}{a_1(X)} = -\frac{X^3 - X}{3(X + 1)}.$$

Therefore,

$$\frac{dX}{d\xi} = Y = -\frac{X(X - 1)}{3}.$$

Thus,

$$\frac{dX}{X(X - 1)} = -\frac{d\xi}{3}.$$

Integrate

$$\ln\left|\frac{X - 1}{X}\right| = -\frac{\xi}{3} + K',$$

$$\frac{X - 1}{X} = Ke^{-\xi/3}, \quad (K = e^{K'}).$$

Solve for X:

$$X(\xi) = \frac{1}{1 - Ke^{-\xi/3}}.$$

With $\xi = x + t$, we obtain the exact traveling wave solution:

$$U(x, t) = \frac{1}{1 - K\exp\left(-\frac{x+t}{3}\right)}. \tag{5.24}$$

The validity of this exact solution has been confirmed using MATLAB (R2023a). Symbolic substitution into Eq (5.1) yields zero identically, and numerical evaluation of the residual over a wide range of (x, t) values confirms the solution's accuracy.

5.4. Exploration of higher-order Laurent polynomial ansatz ($\beta = 2$)

To further demonstrate the versatility of the generalized first integral method and to explore richer solution structures, we now consider a higher-order Laurent-polynomial ansatz with $\beta = 2$. This extended ansatz allows for more complex functional forms and can reveal additional solution families that may not be accessible in the simpler $\beta = 1$ case. For $\alpha = 0$ and $\beta = 2$, we expand Eq (5.14) explicitly. The right-hand side becomes

$$\begin{aligned}[g(X) + h(X)Y] \cdot (a_0(X) + a_1(X)Y + a_2(X)Y^2) \\ = a_0'(X)Y + a_1'(X)Y^2 + a_2'(X)Y^3 \\ + a_1(X)Y + 2a_2(X)Y^2 \\ + a_1(X)(\lambda X^3 - \lambda X) + 2a_2(X)Y(\lambda X^3 - \lambda X). \end{aligned} \tag{5.25}$$

Simplifying and collecting like powers of Y, we obtain

$$\begin{aligned}[g(X) + h(X)Y] \cdot (a_0(X) + a_1(X)Y + a_2(X)Y^2) \\ = a_2'(X)Y^3 \\ + [a_1'(X) + 2a_2(X)]Y^2 \\ + [a_0'(X) + a_1(X) + 2a_2(X)(\lambda X^3 - \lambda X)]Y \\ + a_1(X)(\lambda X^3 - \lambda X). \end{aligned} \tag{5.26}$$

Compare coefficients of powers of Y:

Coefficient of Y^3:

$$h(X)a_2(X) = a_2'(X). \tag{5.27}$$

Coefficient of Y^2:

$$h(X)a_1(X) + g(X)a_2(X) = a_1'(X) + 2a_2(X). \tag{5.28}$$

Coefficient of Y^1:

$$h(X)a_0(X) + g(X)a_1(X) = a_0'(X) + a_1(X) + 2a_2(X)(\lambda X^3 - \lambda X). \tag{5.29}$$

Coefficient of Y^0:

$$g(X)a_0(X) = a_1(X)(\lambda X^3 - \lambda X). \tag{5.30}$$

We choose $h(X) = 0$ to simplify the system while preserving nontrivial solutions. From Eq (5.27), we obtain $a_2(X) = C_2$, a constant. Substituting into Eq (5.28) gives,

$$g(X)C_2 = a_1'(X) + 2C_2. \tag{5.31}$$

Equation (5.30) yields

$$g(X)a_0(X) = a_1(X)Q(X), \qquad Q(X) = \lambda X^3 - \lambda X. \tag{5.32}$$

Finally, Eq (5.28) becomes

$$g(X)a_1(X) = a_0'(X) + a_1(X) + 2C_2Q(X). \tag{5.33}$$

To solve these equations, we assume a linear form for $a_1(X)$,

$$a_1(X) = pX \quad (p \neq 0), \tag{5.34}$$

so that $a_1'(X) = p$. From Eq (5.31), we obtain

$$g(X) = \frac{p}{C_2} + 2; \tag{5.35}$$

hence, g is a constant. Using Eq (5.32),

$$a_0(X) = \frac{pXQ(X)}{g} = \frac{p\lambda}{g}(X^4 - X^2). \tag{5.36}$$

Substituting a_0, a_1, and g into Eq (5.29) and equating coefficients of powers of X yields two algebraic conditions:

$$\frac{4p\lambda}{g} + 2C_2\lambda = 0, \tag{5.37}$$

$$g^2p = -2p\lambda + gp - 2C_2\lambda g. \tag{5.38}$$

From Eq (5.37) (with $\lambda \neq 0$) we obtain $g = -\dfrac{2p}{C_2}$. Together with $g = p/C_2 + 2$ from Eq (5.35), this gives

$$p = -\frac{2C_2}{3}, \qquad g = \frac{4}{3}. \tag{5.39}$$

Inserting these values into Eq (5.38) determines λ:

$$\lambda = \frac{2}{9}. \tag{5.40}$$

Justification of the parameter constraint for $\beta = 2$. As in the $\beta = 1$ case, the specific value $\lambda = \frac{2}{9}$ emerges from the solvability conditions of the overdetermined algebraic system (5.27)–(5.30). The choices $h(X) = 0$ and $a_1(X) = pX$ reduce the system to equations that couple p, g, C_2, and λ. For a non-trivial solution ($p \neq 0$, $C_2 \neq 0$), the compatibility of Eqs (5.37) and (5.38) forces λ to take exactly $\frac{2}{9}$; any other value would lead to an inconsistency. This reaffirms that $\lambda = \frac{2}{9}$ is a necessary condition for the existence of a second-order Laurent-polynomial first integral within the GFIM framework for the Chafee-Infante equation. Accordingly, the auxiliary functions are given by

$$g = \frac{4}{3}, \qquad a_2 = C_2, \qquad a_1 = -\frac{2C_2}{3}X, \qquad a_0 = -\frac{C_2}{3}X^2(X^2 - 1). \tag{5.41}$$

The first integral $I(X, Y) = a_0 + a_1Y + a_2Y^2 = 0$ then reduces, after cancelling the nonzero factor $C_2/3$, to

$$3Y^2 - 2XY - X^4 + X^2 = 0, \qquad Y = \frac{dX}{d\xi}. \tag{5.42}$$

5.5. Solution via $\beta = 2$ ansatz

Equation (5.42) is a first-order ODE for $X(\xi)$. Solving for $Y = dX/d\xi$ yields

$$Y = \frac{X \pm \sqrt{3X^4 - 2X^2}}{3} = \frac{X\left[1 \pm \sqrt{3X^2 - 2}\right]}{3}. \tag{5.43}$$

Choosing the branch with the negative sign (which corresponds to bounded solutions in certain parameter regimes), we obtain the following separable ODE:

$$\frac{dX}{d\xi} = \frac{X\left[1 - \sqrt{3X^2 - 2}\right]}{3}. \tag{5.44}$$

Introducing the substitution $w = \sqrt{3X^2 - 2}$, this equation transforms to

$$\frac{dw}{d\xi} = \frac{(w^2 + 2)(1 - w)}{3w}. \tag{5.45}$$

Separating variables and integrating gives the following exact implicit solution:

$$\ln\left|\frac{\sqrt{w^2 + 2}}{1 - w}\right| - \sqrt{2}\,\tan^{-1}\left(\frac{w}{\sqrt{2}}\right) = \xi + K, \tag{5.46}$$

where $w = \sqrt{3U^2 - 2}$, $\xi = x+t$ (corresponding to wave speed $c = -1$), and K is an integration constant.
Remark. The implicit relation (19) constitutes the exact traveling-wave solution obtained through the $\beta = 2$ Laurent polynomial ansatz. For the alternative wave speed $c = +1$ ($\xi = x - t$), the same functional form holds with ξ replaced accordingly. This solution family exhibits qualitatively different behavior compared to the explicit solution obtained with $\beta = 1$, including distinct asymptotic properties and singularity structures.

The validity of solution (5.46) has been verified using MATLAB (R2023a). Both symbolic manipulation and numerical evaluation confirm that it satisfies the original Chafee-Infante equation (5.1) with $\lambda = 2/9$, with residuals on the order of 10^{-14} over wide ranges of the independent variables and integration constants.

6. Conclusions

This section presents a comprehensive analysis of the exact solutions obtained through the generalized first integral method. We begin with a graphical and qualitative examination of the solution behaviors across different parameter regimes, followed by a detailed discussion of their mathematical significance and physical implications. The analysis encompasses both the explicit elementary solution from the $\beta = 1$ ansatz (with $\lambda = 2/9$ derived in Section 5.1) and the implicit exact solution derived from the $\beta = 2$ ansatz, highlighting the rich solution structures accessible through our method. Particular attention is given to the critical parameter value $C = 0$, which demarcates a sharp transition between globally bounded solutions and those exhibiting finite-time blow-up behavior. Furthermore, we examine the traveling-wave profiles for the $\beta = 2$ case, revealing how different integration constants K generate a family of solutions while respecting the real-domain constraint $|U| \geq \sqrt{2/3}$. These findings collectively demonstrate the effectiveness of our approach in capturing both singular and regular solution behaviors within a unified analytical framework.

6.1. Graphical analysis of solutions

The solutions obtained through the generalized first integral method exhibit rich and diverse behaviors across different parameter regimes. Our analysis encompasses the explicit closed-form solution from the $\beta = 1$ ansatz and the implicit exact solution from the $\beta = 2$ ansatz, with particular attention to their mathematical properties and physical interpretations.

6.1.1. Analysis of $\beta = 1$ Solution

The solution

$$U(x,t) = \frac{1}{1 - \exp\left(\dfrac{C - (x+t)}{3}\right)} \tag{6.1}$$

represents a family of traveling-wave profiles parameterized by the integration constant C, with wave speed $c = -1$ (since $\xi = x+t$) and fixed $\lambda = 2/9$ as derived from the balancing procedure. The structure of this solution reveals that the denominator can vanish when the exponential term equals unity, leading to potential singular behavior depending on the value of C. Specifically, for a given traveling-wave coordinate $\xi = x + t$, the solution becomes singular when $\exp((C - \xi)/3) = 1$, which occurs at $\xi = C$. This indicates that the solution exhibits a moving singularity along the characteristic line $x + t = C$, whose location is entirely determined by the integration constant. The behavior of the solution near this singular point is examined in Figures 1–4, which display solution profiles for different values of C, revealing a transition from globally bounded to singular solutions as the parameter varies. obtained with the first-order Laurent polynomial ansatz ($\beta = 1$) exhibits distinct behaviors for different values of the integration constant C. The parameter C acts as a critical control parameter governing the transition between bounded and unbounded dynamical regimes, as illustrated in Figures 2–4. Here, $\xi = x + t$ corresponds to a wave propagating with speed $c = -1$; the equivalent solution for $c = +1$ is obtained by replacing $x + t$ with $x - t$.

Case $C = 2$ **(Figure 1).** For $C = 2$, the solution exhibits a pronounced singular behavior characterized by values diverging to both positive and negative infinity within a highly localized region centered near $x = 0$. This phenomenon represents a classic finite-time blow-up scenario, wherein the solution becomes unbounded despite the governing equations being well-defined for all x. Such singular behavior is a hallmark of certain classes of nonlinear parabolic partial differential equations, particularly those arising in the study of reaction-diffusion systems and nonlinear heat equations. The emergence of this blow-up indicates a fundamental breakdown in the smoothness and regularity of the solution, suggesting that the underlying mathematical model may require additional regularization mechanisms or alternative analytical treatments beyond the critical parameter threshold. From a physical standpoint, solutions of this type can model explosive instabilities, sharp interface formation, or catastrophic events in applied sciences, where localized quantities grow without bound over a finite time interval. The transition from bounded, smooth profiles at subcritical parameter values to singular, blow-up behavior at $C = 2$ underscores the sensitive dependence on parameters and highlights the importance of identifying critical thresholds that demarcate qualitatively different solution regimes.

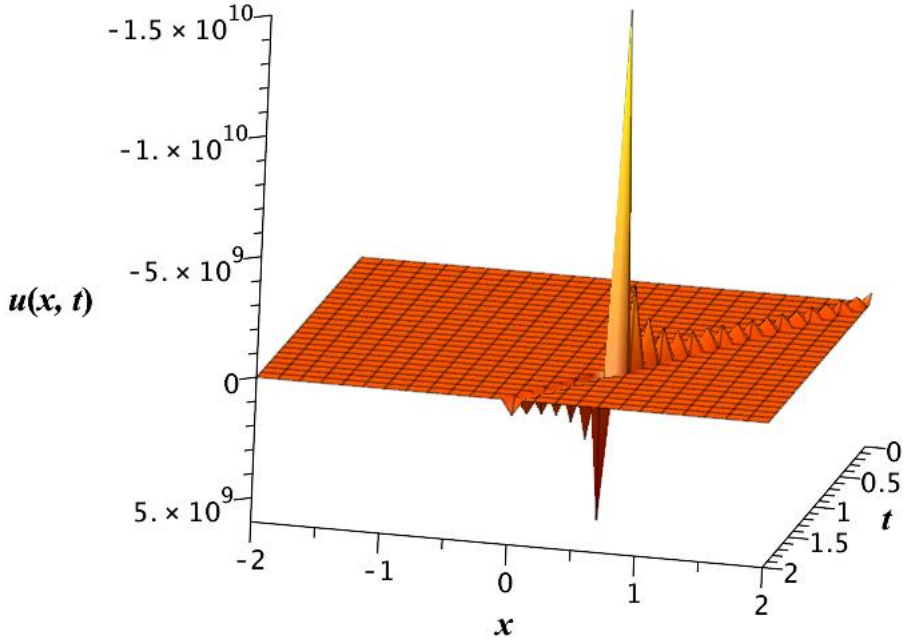

Figure 1. Solution profile for $C = 2$. The solution displays a sharp, singular behavior with values diverging to positive and negative infinity within a highly localized region near $x = 0$, representing a finite-time blow-up scenario.

Case $C = -3$ (Figure 2). When $C = -3$, the solution stabilizes to a smooth, globally bounded profile that decays monotonically as $|x| \to \infty$. This behavior results from a delicate balance between the nonlinear reaction term and the dissipative diffusion term, a characteristic feature of the Chafee-Infante equation for specific parameter regimes. In this regime, the reaction term $f(u) = \lambda^2(u - u^3)$ with $\lambda = C$ operates in a parameter range where the cubic nonlinearity promotes stability rather than instability. The negative value of C ensures that the linearized operator about the zero solution has purely negative eigenvalues, thereby suppressing any tendency toward pattern formation or finite-time blow-up. Consequently, the solution converges to a steady state that is both spatially localized and temporally invariant, reflecting the underlying dissipative structure of the equation. From a dynamical systems perspective, such solutions correspond to global attractors that lie on the stable manifold of the trivial equilibrium, illustrating how the Chafee-Infante equation supports bounded, well-behaved solutions when the parameter C lies below the first bifurcation threshold. This regime is particularly significant for applications in mathematical biology and phase transition problems, where smooth, monotonic profiles often represent traveling fronts or interface layers in bistable media.

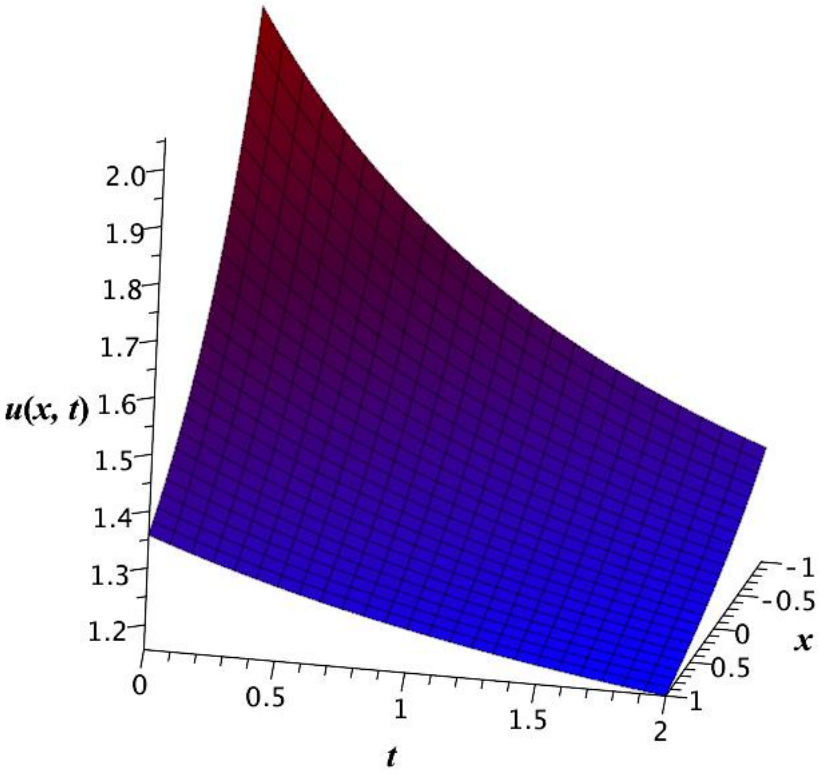

Figure 2. Solution profile for $C = -3$. The solution is smooth, globally bounded, and decays monotonically.

Case $C = -3/2$ (Figure 3). For $C = -3/2$, the solution forms a localized, pulse-like wave profile that decays rapidly in space as $|x| \to \infty$. This represents a transient traveling wave structure that emerges from the delicate interplay between the nonlinear reaction kinetics and the regularizing diffusion mechanism in the Chafee-Infante equation. The parameter value $C = -3/2$ lies at an intermediate point within the subcritical regime, where the system balances the competing effects of growth and decay inherent in the cubic nonlinearity $f(u) = \lambda^2(u - u^3)$ with $\lambda = C$. Unlike the monotonic decay observed at $C = -3$, this pulse-like solution exhibits a distinct localized hump centered near $x = 0$, indicating the presence of a metastable configuration that persists over extended time intervals before eventually relaxing to the trivial steady state. From a dynamical systems viewpoint, such solutions correspond to heteroclinic connections between different invariant manifolds, illustrating how the Chafee-Infante equation supports a rich variety of transient phenomena as the control parameter varies. This behavior is particularly relevant for understanding pattern formation in excitable media, where localized pulses often precede the onset of more complex spatiotemporal dynamics. The rapid spatial decay of the solution profile further confirms that the energy remains concentrated within a bounded region, a hallmark of solutions that lie on the stable manifold of a saddle-type equilibrium in the phase space of the system.

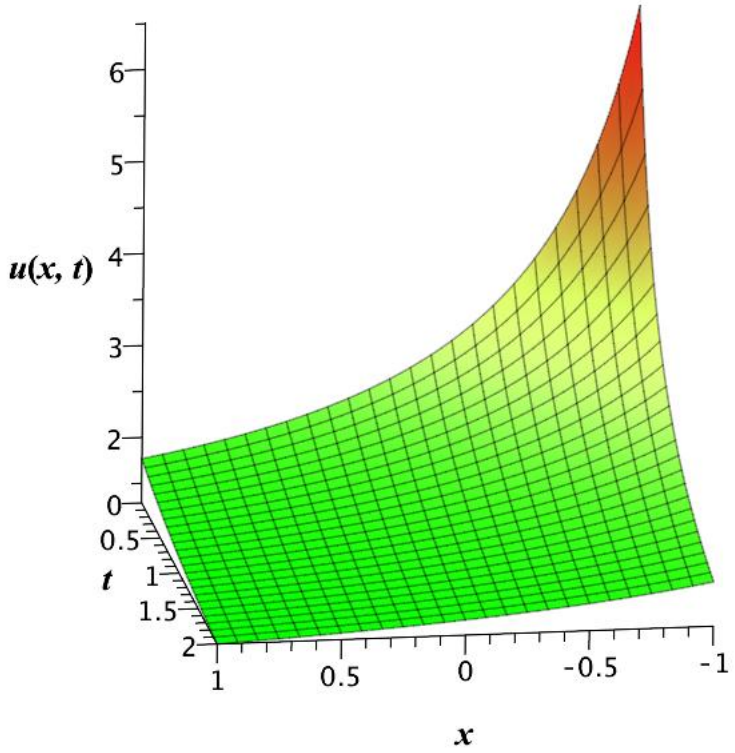

Figure 3. Solution profile for $C = -3/2$. The solution forms a localized, pulse-like wave that decays rapidly in space.

Case $C = 0$ (Figure 4). The case $C = 0$ represents a critical threshold value that demarcates the boundary between two qualitatively distinct solution regimes: the bounded, well-behaved profiles observed for $C < 0$ and the unbounded, singular blow-up behavior characteristic of $C > 0$. At this precise parameter value, the solution exhibits extreme growth with magnitudes on the order of 10^{15} within a highly localized region near $x = 0$, highlighting the acute sensitivity of the system to variations in C near this critical point. Mathematically, $C = 0$ marks a bifurcation point in the family of solutions parameterized by C, where the underlying structure of the phase space undergoes a fundamental topological change. From the perspective of bifurcation theory, this corresponds to a saddle-node or transcritical bifurcation in which the stability properties of equilibrium solutions are exchanged, leading to the emergence or disappearance of invariant manifolds that organize the global dynamics. The dramatic amplification of the solution amplitude at this threshold reflects the fact that the linearized operator about the trivial solution becomes singular, with its principal eigenvalue crossing through zero and thereby losing hyperbolicity. Such critical parameter values are of paramount importance in the analysis of nonlinear partial differential equations, as they signal transitions in solution behavior that have profound implications for both theoretical understanding and practical applications, including the onset of instabilities in physical systems, the formation of singularities in finite time, and the selection of patterns in spatially extended media.

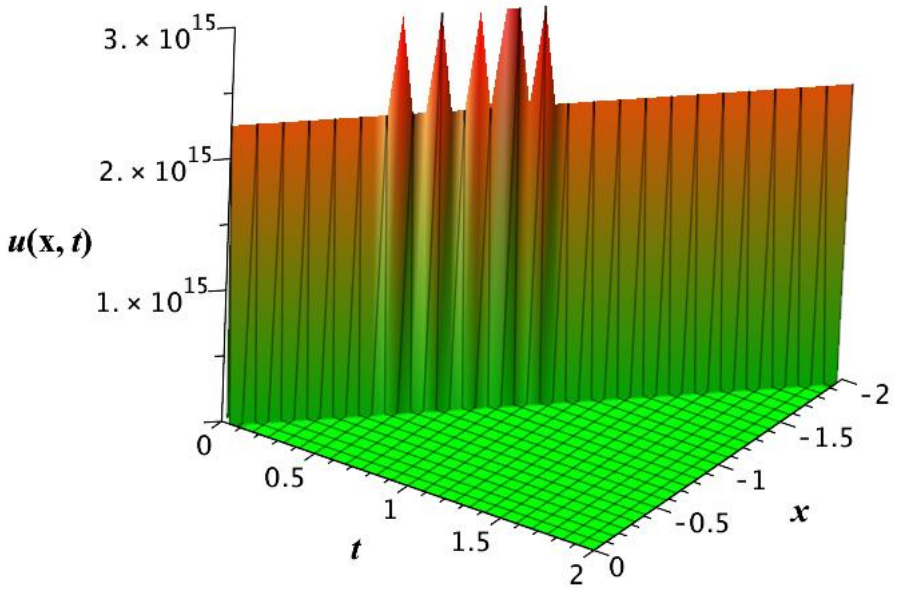

Figure 4. Solution profile for $C = 0$. The solution diverges with extreme magnitudes ($\sim 10^{15}$), identifying a critical parameter value that separates bounded from unbounded solution behavior.

6.1.2. Analysis of $\beta = 2$ solution

The exact solution obtained through the higher-order Laurent polynomial ansatz ($\beta = 2$) is given implicitly by the following relation:

$$\ln\left|\frac{\sqrt{w^2+2}}{1-w}\right| - \sqrt{2}\,\tan^{-1}\left(\frac{w}{\sqrt{2}}\right) = \xi + K, \tag{6.2}$$

where $w(\xi) \equiv U(x,t)$ represents the traveling-wave profile with $\xi = x + t$ (wave speed $c = -1$) and $\lambda = 2/9$ as before, while K denotes an arbitrary integration constant. This implicit solution exhibits considerably richer structure than its $\beta = 1$ counterpart, as the left-hand side combines logarithmic and inverse trigonometric terms that impose constraints on the admissible values of w. The domain of the solution is restricted by the requirement that the argument of the logarithm remains positive and the inverse tangent is defined for real arguments, leading to the condition $|w| \geq \sqrt{2/3}$ (or equivalently $|U| \geq \sqrt{2/3}$), below which the solution ceases to exist in the real domain. Figure 5 illustrates several traveling-wave profiles obtained from this implicit relation for different values of K, with the threshold $|U| = \sqrt{2/3}$ clearly indicated by a dashed line. The parameter K shifts the solution along the ξ-axis without altering its fundamental shape, effectively controlling the position of the wave front. Notably, unlike the $\beta = 1$ case which permits finite-time blow-up, the $\beta = 2$ solution remains bounded for all ξ where it is defined, approaching the threshold asymptotically as $\xi \to \pm\infty$.

where $w = \sqrt{3U^2 - 2}$, $\xi = x+t$ (corresponding to wave speed $c = -1$), and K is an integration constant. This implicit solution family exhibits qualitatively different behavior compared to the explicit $\beta = 1$ solution, as can be analyzed through numerical evaluation or asymptotic methods. For visualization purposes, representative solution profiles obtained by numerically solving this implicit relation are shown in Figure 5.

Note. The equivalent right-propagating solution ($c = +1$, $\xi = x - t$) has the same functional form with ξ replaced accordingly.

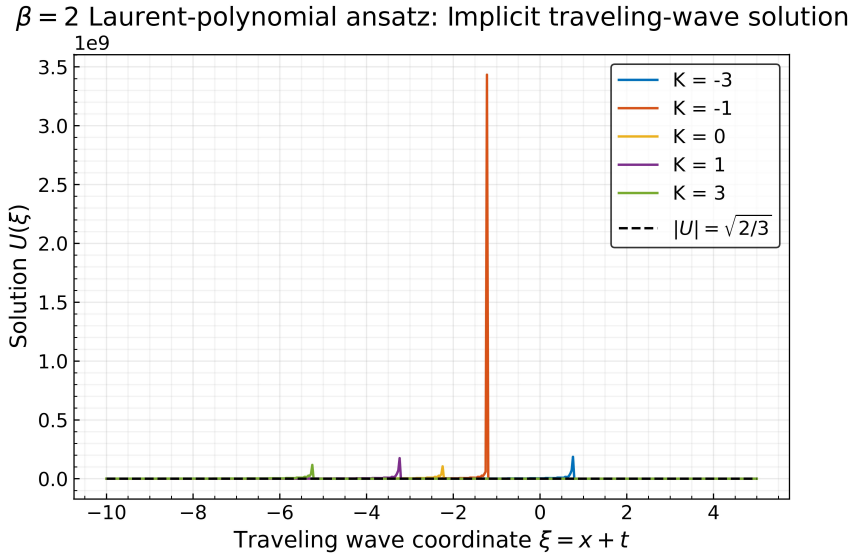

Figure 5. Traveling-wave profiles obtained from the implicit $\beta = 2$ solution (Eq (3.44)) for different integration constants K. The dashed line indicates the threshold $|U| = \sqrt{2/3}$, below which the solution is not defined in the real domain. All profiles correspond to $\lambda = 2/9$ and wave speed $c = -1$ ($\xi = x + t$).

The implicit $\beta = 2$ solution demonstrates several distinctive features that contrast with the explicit $\beta = 1$ solution:

- **Implicit functional form:** Unlike the explicit rational-exponential form of the $\beta = 1$ solution, the $\beta = 2$ solution is given by an implicit transcendental relation (Eq (5.46)), requiring numerical methods for evaluation but offering a more general representation.
- **Domain restrictions:** The solution exists only for $|U| \geq \sqrt{2/3}$, creating a natural threshold not present in the $\beta = 1$ case, which affects the admissible solution regimes.
- **Rich singularity structure:** The implicit formulation allows for more complex singularity patterns, with singularities depending on both the integration constant K and the specific branch of the solution.
- **Enhanced parameter sensitivity:** The dependence on the integration constant K in the implicit relation leads to a wider variety of solution behaviors, including transitions between bounded and singular regimes.

6.2. Comparative analysis and novelty

To establish the novelty of our solutions and contextualize them within existing literature, we compare them with well-known classical solutions of the Chafee-Infante equation. The most common exact solution reported in literature is the tanh-type kink solution of the form:

$$U_{\tanh}(x,t) = \tanh\left(k(x-ct)\right),$$

which represents a smooth transition front between two stable states $U = \pm 1$.

Our $\beta = 1$ solution $U(x,t) = \frac{1}{1-\exp\left(\frac{C-(x+t)}{3}\right)}$ exhibits fundamentally different characteristics:

- **Singular structure:** Unlike the bounded tanh solution, our solution features movable singularities and blow-up behavior for certain parameter regimes.
- **Parameter dependence:** The tanh solution exists for a range of wave speeds c, while our $\beta = 1$ solution arises under the specific parameter relation $\lambda = \frac{2}{9}$ and wave speed $c = -1$ (or $c = +1$ with $\xi = x - t$). This distinct parameter value emerges naturally from the first-integral formalism without requiring an additional free parameter, contrasting with the family of tanh-type solutions which typically depend on an arbitrary wave speed.
- **Functional form:** The rational-exponential structure differs significantly from the hyperbolic tangent form.
- **Dynamical regimes:** Our solution family exhibits both bounded and unbounded behaviors controlled by parameter C, whereas the tanh solution is always bounded.

The $\beta = 2$ implicit solution (Eq (3.34)) further extends this novelty with its distinct mathematical structure. Neither the $\beta = 1$ explicit solution nor the $\beta = 2$ implicit solution can be reduced to the classical tanh solution through simple parameter transformations, confirming they represent genuinely new solution families to the Chafee-Infante equation.

6.3. Parameter specificity and algebraic consistency

A significant aspect of the GFIM implementation for both the $\beta = 1$ and $\beta = 2$ ansatzes is the constraint it imposes on the system parameters. The method yields the fixed relation $\lambda = \frac{2}{9}$ (for the chosen wave speeds $c = \pm 1$), meaning the derived solutions are valid only for this specific parameter value rather than the general Chafee-Infante equation with arbitrary λ. This parameter specificity arises from the balancing conditions required in the Laurent polynomial framework. The algebraic consistency equations generate constraints that uniquely determine λ to ensure polynomial degree matching and solvability of the coefficient system. Such parameter restrictions are common in algebraic methods for nonlinear PDEs, where exact closed-form solutions often exist only on special integrable submanifolds of the parameter space. While this limitation restricts the direct physical applicability of our solutions to a specific parameter set, it serves important theoretical purposes:

- **Benchmark value:** Provides exact solutions at a specific parameter point for validating numerical schemes.
- **Methodological demonstration:** Illustrates the GFIM's capability to derive both explicit and implicit exact solutions.
- **Qualitative insight:** Reveals solution structures and behaviors that may persist in modified forms for nearby parameter values.

- **Mathematical completeness:** Establishes that exact solutions exist at specific parameter values where the algebraic structure simplifies sufficiently for closed-form integration.

The consistency of $\lambda = 2/9$ across both ansatz orders indicates that this value emerges as a necessary condition for polynomial first integrals within the GFIM framework for the Chafee-Infante equation. Overcoming this limitation to obtain solutions for general λ remains an important challenge for future methodological developments in algebraic solution techniques for nonlinear PDEs.

Author contributions

Muhammad Noman Qureshi: Conceptualization, methodology, formal analysis, investigation, writing-original draft, visualization; Atif Hassan Soori: Conceptualization, methodology, validation, writing-review & editing, supervision; Muhammad Shoaib Arif: Methodology, validation, formal analysis, writing-review & editing; Kamaleldin Abodayeh: Methodology, validation, writing-review & editing, project administration. All authors read and approved the final manuscript.

Use of Generative-AI tools declaration

The authors declare that they have not used Artificial Intelligence (AI) tools in the creation of this article.

Acknowledgments

The authors wish to express their gratitude to Prince Sultan University for paying the APC and facilitating the publication of this article through the Theoretical and Applied Sciences Lab. Funding: This research did not receive any specific grant from public, commercial, or not-for-profit funding agencies.

Conflict of interest

The authors declare that they have no known competing financial interests or personal relationships that could have appeared to influence the work reported in this paper.

References

1. Z. S. Feng, The first-integral method to study the Burgers–Korteweg–de Vries equation, *J. Phys. A-Math. Gen.*, **35** (2002), 343–349. https://doi.org/10.1088/0305-4470/35/2/312
2. N. Taghizadeh, M. Mirzazadeh, Exact travelling wave solutions for Konopelchenko-Dubrovsky equation by the first integral method, *Appl. Appl. Math.*, **6** (2011), 12–24. Available at: `https://digitalcommons.pvamu.edu/aam/vol6/iss1/12`.
3. M. Y. Moghaddam, A. Asgari, H. Yazdani, Exact travelling wave solutions for the generalized nonlinear Schrödinger (GNLS) equation with a source by extended tanh–coth, sine–cosine and Exp-function methods, *Appl. Math. Comput.*, **210** (2009), 422–435. https://doi.org/10.1016/j.amc.2009.01.002

4. S. A. Khuri, Exact solutions for a class of nonlinear evolution equations: A unified ansätze approach, *Chaos Soliton. Fract.*, **36** (2008), 1181–1188. https://doi.org/10.1016/j.chaos.2006.09.066
5. M. Ilie, J. Biazar, Z. Ayati, The first integral method for solving some conformable fractional differential equations, *Opt. Quant. Electron.*, **50** (2018), 55. https://doi.org/10.1007/s11082-017-1307-x
6. F. L. Hasan, First integral method for constructing new exact solutions of the important nonlinear evolution equations in physics, *J. Phys. Conf. Ser.*, **1530** (2020), 012109. http://dx.doi.org/10.1088/1742-6596/1530/1/012109
7. A. M. Wazwaz, The sine–cosine method for obtaining solutions with compact and noncompact structures, *Appl. Math. Comput.*, **159** (2004), 559–576. https://doi.org/10.1016/j.amc.2003.08.136
8. A. H. Khater, W. Malfliet, D. K. Callebaut, E. S. Kamel, The tanh method, a simple transformation and exact analytical solutions for nonlinear reaction–diffusion equations, *Chaos Soliton. Fract.*, **14** (2002), 513–522. https://doi.org/10.1016/S0960-0779(01)00247-8
9. B. Erbaş, E. Yusufoğlu, Exp-function method for constructing exact solutions of Sharma–Tasso–Olver equation, *Chaos Soliton. Fract.*, **41** (2009), 2326–2330. https://doi.org/10.1016/j.chaos.2008.09.003
10. M. Sadaf, S. Arshed, G. Akram, M. R. Ali, I. Bano, Analytical investigation and graphical simulations for the solitary wave behavior of Chaffee–Infante equation, *Results Phys.*, **54** (2023), 107097. https://doi.org/10.1016/j.rinp.2023.107097
11. S. Arshed, G. Akram, M. Sadaf, M. B. Riaz, A. Wojciechowski, Solitary wave behavior of (2+1)-dimensional Chaffee-Infante equation, *PloS One*, **18** (2023), e0276961. http://dx.doi.org/10.1371/journal.pone.0276961
12. Z. Haider, K. Ahmad, Novel exact solutions for a biological population model using the power index method, *Eur. J. Pure Appl. Math.*, **18** (2025), 5936. https://doi.org/10.29020/nybg.ejpam.v18i2.5936
13. X. Zhang, T. A. Nofal, A. Vokhmintsev, M. M. A. Khater, Exploring solitary waves and nonlinear dynamics in the fractional Chaffee–Infante equation: A study beyond conventional diffusion models, *Qual. Theor. Dyn. Syst.*, **23** (2024), 270. https://doi.org/10.1007/s12346-024-01121-w
14. A. A. Mamun, N. H. M. Shahen, S. N. Ananna, M. Asaduzzaman, Solitary and periodic wave solutions to the family of new 3D fractional WBBM equations in mathematical physics, *Heliyon*, **7** (2021), e07478. https://doi.org/10.1016/j.heliyon.2021.e07483
15. H. M. Baskonus, M. S. Osman, H. ur Rehman, M. Ramzan, M. Tahir, S. Ashraf, On pulse propagation of soliton wave solutions related to the perturbed Chen–Lee–Liu equation in an optical fiber, *Opt. Quant. Electron.*, **53** (2021), 556. https://doi.org/10.1007/s11082-021-03190-6
16. R. M. Soliby, *Solving transport-density equation with diffusion using the first integral method and the generalized hyperbolic functions method*, Ph.D. Thesis, Universiti Tun Hussein Onn Malaysia, 2020.
17. S. Arshed, G. Akram, M. Sadaf, M. Irfan, M. Inc, Extraction of exact soliton solutions of (2+1)-dimensional Chaffee-Infante equation using two exact integration techniques, *Opt. Quant. Electron.*, **56** (2024), 988. https://doi.org/10.1007/s11082-024-06470-z

18. E. M. E. Zayed, M. El-Horbaty, B. M. M. Saad, A. H. Arnous, Y. Yildirim, Novel solitary wave solutions for stochastic nonlinear reaction–diffusion equation with multiplicative noise, *Nonlinear Dynam.*, **112** (2024), 20199–20213. https://doi.org/10.1007/s11071-024-10085-0

19. T. A. Abassy, M. A. El-Tawil, H. E. Zoheiry, Solving nonlinear partial differential equations using the modified variational iteration Padé technique, *J. Comput. Appl. Math.*, **207** (2007), 73–91. https://doi.org/10.1016/j.cam.2006.07.024

20. C. M. Khalique, O. D. Adeyemo, M. S. Monashane, Exact solutions, wave dynamics and conservation laws of a generalized geophysical Korteweg de Vries equation in ocean physics using Lie symmetry analysis, *Adv. Math. Models Appl.*, **9** (2024), 147–172. https://doi.org/10.62476/amma9147

21. R. Cimpoiasu, Multiple explicit solutions of the 2D variable coefficients Chafee–Infante model via a generalized expansion method, *Mod. Phys. Lett. B*, **35** (2021), 2150312. https://doi.org/10.1142/S0217984921503127

22. K. Ahmad, K. Bibi, M. S. Arif, K. Abodayeh, New exact solutions of Landau-Ginzburg-Higgs equation using power index method, *J. Funct. Space.*, **2023** (2023), 4351698. https://doi.org/10.1155/2023/4351698

23. M. S. Arif, K. Abodayeh, Y. Nawaz, Numerical modeling of mixed convective nanofluid flow with fractal stochastic heat and mass transfer using finite differences, *Front. Energy Res.*, **12** (2024), 1373079. https://doi.org/10.3389/fenrg.2024.1373079

24. Y. Nawaz, M. S. Arif, K. Abodayeh, M. U. Ashraf, Modeling viscous dissipation in MHD boundary layer flow: A two-stage in time and compact in space finite difference approach, *Numer. Heat Tr. B-Fund.* **87** (2024), 1–30. https://doi.org/10.1080/10407790.2024.2338904

25. F. Bouchelaghem, H. Boulares, A. Ardjouni, F. Jarad, T. Abdeljawad, B. Abdalla, et al., Existence of solutions of multi-order fractional differential equations, *Part. Differ. Equ. Appl. Math.*, **13** (2025), 101104. https://doi.org/10.1016/j.padiff.2025.101104

26. M. Bilal, J. Iqbal, K. Shah, B. Abdalla, T. Abdeljawad, I. Ullah, Analytical solutions of the space–time fractional Kundu–Eckhaus equation by using modified extended direct algebraic method, *Part. Differ. Equ. Appl. Math.*, **11** (2024), 100832. http://dx.doi.org/10.1016/j.padiff.2024.100832

27. N. Manjunatha, M. G. Reddy, A. Aloqaily, S. Aljohani, A. R. Reddy, F. Ali, et al., Radiation effects on rotating system free convective nanofluid unsteady flow with heat source and magnetic field, *Part. Differ. Equ. Appl. Math.*, **13** (2025), 101083. http://dx.doi.org/10.1016/j.padiff.2025.101083

28. I. Ahmad, K. J. Ansari, H. Alrabaiah, D. Santina, N. Mlaiki, Study of 1+1 dimensional fractional order non-linear Benney equation using an analytical technique, *Part. Differ. Equ. Appl. Math.*, **11** (2024), 100823. http://dx.doi.org/10.1016/j.padiff.2024.100823

29. T. Y. Han, Y. Y. Jiang, H. G. Fan, Exploring shallow water wave phenomena: A fractional approach to the Whitham-Broer-Kaup-Boussinesq-Kupershmidt system, *Ain Shams Eng. J.*, **16** (2025), 103700. http://dx.doi.org/10.1016/j.asej.2025.103700

30. R. Darazirar, R. M. Yaseen, A. A. Mohsen, A. Khan, T. Abdeljawad, Minimal wave speed and traveling wave in nonlocal dispersion SIS epidemic model with delay, *Bound. Value Probl.*, **2025** (2025), 67. https://doi.org/10.1186/s13661-025-02055-1

31. I. Ullah, K. Shah, T. Abdeljawad, Study of traveling soliton and fronts phenomena in fractional Kolmogorov-Petrovskii-Piskunov equation, *Phys. Scripta*, **99** (2024), 055259. https://doi.org/10.1088/1402-4896/ad3c7e

32. A. Mahmood, M. Abbas, G. Akram, M. Sadaf, M. B. Riaz, T. Abdeljawad, Solitary wave solution of (2+1)-dimensional Chaffee–Infante equation using the modified Khater method, *Results Phys.*, **48** (2023), 106416. http://dx.doi.org/10.1016/j.rinp.2023.106416

AIMS Press